nature COMMUNICATIONS

ARTICLE

https://doi.org/10.1038/s41467-022-31498-8 OPEN

Hydroxyl radicals dominate reoxidation of oxide-derived Cu in electrochemical CO_2 reduction

Shijia Mu[1], Honglei Lu[1], Qianbao Wu[1], Lei Li[1], Ruijuan Zhao[1], Chang Long[1✉] & Chunhua Cui[1✉]

$Cu^{\delta+}$ sites on the surface of oxide-derived copper (OD-Cu) are of vital importance in electrochemical CO_2 reduction reaction (CO_2RR). However, the underlying reason for the dynamically existing $Cu^{\delta+}$ species, although thermodynamically unstable under reductive CO_2RR conditions, remains uncovered. Here, by using electron paramagnetic resonance, we identify the highly oxidative hydroxyl radicals ($OH^•$) formed at room temperature in HCO_3^- solutions. In combination with in situ Raman spectroscopy, secondary ion mass spectrometry, and isotope-labelling, we demonstrate a dynamic reduction/reoxidation behavior at the surface of OD-Cu and reveal that the fast oxygen exchange between HCO_3^- and H_2O provides oxygen sources for the formation of $OH^•$ radicals. In addition, their continuous generations can cause spontaneous oxidation of Cu electrodes and produce surface CuO_x species. Significantly, this work suggests that there is a "seesaw-effect" between the cathodic reduction and the $OH^•$-induced reoxidation, determining the chemical state and content of $Cu^{\delta+}$ species in CO_2RR. This insight is supposed to thrust an understanding of the crucial role of electrolytes in CO_2RR.

[1] Molecular Electrochemistry Laboratory, Institute of Fundamental and Frontier Sciences, University of Electronic Science and Technology of China, Chengdu 610054, China. ✉email: longch@uestc.edu.cn; chunhua.cui@uestc.edu.cn

Conversion of CO_2 into value-added chemicals through renewable electricity-powered electrochemical CO_2 reduction reaction (CO_2RR) has been recognized as a promising strategy to achieve "carbon-neutral"[1–3]. Oxide-derived copper (OD-Cu) has been proven as a group of efficient electrocatalysts for CO_2RR, especially for multi-carbon products (C_{2+})[4–6]. The precise mechanism remains unknown and different views have been proposed[7–14]. Specifically, both experiments and theoretical calculations demonstrated that the $Cu^{\delta+}/Cu^0$ interface can activate the inert CO_2 molecules and promote CO-CO coupling[10,11]. To regulate the selectivity of C_{2+} products, many efficient OD-Cu catalysts with characteristic $Cu^{\delta+}$ sites have been achieved through constructing various oxidized pre-catalysts or employing CO_2-pulsed electrolysis[7–9,12].

Thermodynamically, CuO_x phases should be removed under the CO_2RR conditions thereby the loss of the active $Cu^{\delta+}$ species[15]. While some studies have demonstrated the reduction of CuO_x phases to metallic Cu during CO_2RR[16–20]. Interestingly, despite these, the $Cu^{\delta+}$ species has been frequently detected in CO_2RR[8,9,21–23]. This puzzling phenomenon leads to divergent views of the presence of $Cu^{\delta+}$ species. Cuenya et al. demonstrated that the O_2 plasma-treated CuO_x is resistant to reduction[24]. Yu et al. found that in situ generated CO_2RR intermediates on the surface of OD-Cu stabilize $Cu^{\delta+}$ species[8]. Chen et al. pointed out that the chemical states of Cu are associated with the oxidation caused by an uncertain oxidative species in the electrolytes[25–27]. We took the view that the $Cu^{\delta+}$ species should be dynamically existing, and we propose that the redox conditions provided by electrochemical cathodic reduction and oxidative species in electrolytes should be crucial. Understanding the reduction/reoxidation behavior of OD-Cu in commonly used CO_2-saturated $KHCO_3$ electrolytes is a grand challenge but vital to identifying what is the oxidative species.

Here, using in situ Raman spectroscopy, we observe the rapid reoxidation phenomenon of Cu to Cu_2O species within a very short time scale (10 s) upon stopping the cathodic potential, and we record the dynamically existing $Cu^{\delta+}$ species at the surface of OD-Cu during the CO_2RR. We further identify that the rapid reoxidation is caused by strongly oxidative $OH^•$ radicals existing in $KHCO_3$ solutions, by using electron paramagnetic resonance (EPR). With the isotope-labeling technique, we point out that the $OH^•$ radicals are generated from both HCO_3^- and H_2O upon oxygen exchange in HCO_3^- aqueous solutions at room temperature. In addition, owing to the continuous generation of $OH^•$ radicals, we observe higher degrees of oxidizing corrosion of Cu electrodes in CO_2- or Ar-saturated $KHCO_3$ solution under open circuit potential (OCP) relative to those electrolytes without $OH^•$ radicals, giving a hint of oxidative $KHCO_3$ electrolytes. This work demonstrates unexpected $OH^•$ radicals as the oxidative species, and it guides the fundamental understanding of the origin of $Cu^{\delta+}$ species in CO_2RR.

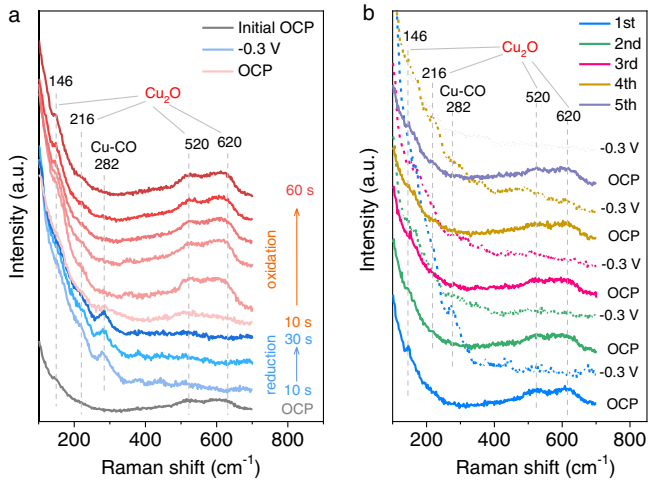

Fig. 1 In situ Raman spectra of OD-Cu electrodes in CO_2-saturated 0.5 M $KHCO_3$. **a** Real-time Raman spectra of surface Cu_2O species at −0.3 V_{RHE} and subsequently at open circuit potential (OCP). **b** Raman spectra under loop tests with a reduction potential at −0.3 V_{RHE} for 10 s and reoxidation potential at OCP for 20 s.

Results

Dynamic reduction/reoxidation behavior. To enhance in situ Raman signals, a surface roughened OD-Cu electrode was selected as a model catalyst for this study[4,28]. It was prepared via depositing the micro-nano Cu particles onto the surface of the Cu mesh substrate (Supplementary Fig. 1), by using a modified electrodeposition method[29]. The as-prepared Cu electrodes show a mainly metallic Cu state, with surfaces being oxidized to Cu_2O phases owing to the exposure to air after electrodeposition and $KHCO_3$ electrolytes before applying potentials for CO_2RR (Supplementary Fig. 1).

We implemented potential-dependent Raman spectra to investigate the stability of surface Cu_2O species under cathodic potentials in CO_2-saturated 0.5 M $KHCO_3$ solution (Supplementary Fig. 2). The vibration bands of surface Cu_2O were observed at ~216, ~520, and ~620 cm^{-1} at >0.0 V versus reversible hydrogen electrode (V_{RHE})[28,30,31]. While, at <−0.2 V_{RHE}, the typical Cu_2O signals disappear, indicating the surface Cu^+ species was reduced to metallic Cu. This result is supported by the prediction of the Pourbaix diagram for Cu and the previous reports[15–20]. In addition, the peaks at 282, 360, 2070–2100 cm^{-1} are related to the frustrated ρ(Cu–C–O) rotational mode, ν(Cu–CO) stretching mode, and intramolecular C≡O stretching vibration of CO intermediates, respectively. The bands at 2820–2950 cm^{-1} are assigned to the -CH_x stretching regions[30,31] from 0.2 to −0.6 V_{RHE} (Fig. 1a, b and Supplementary Figs. 2–4), demonstrating the initiation of CO_2RR. Thus, to reduce surface Cu_2O to metallic Cu (Supplementary Figs. 2 and 5) and to avoid the reconstruction of Cu at very negative potentials during CO_2RR[18,32], a moderate reduction potential of −0.3 V_{RHE} was chosen for further Raman study.

The reoxidation of OD-Cu surface was investigated via real-time Raman test, by applying a reduction potential at −0.3 V_{RHE} for 30 s firstly, and then switching to OCP for 60 s. The spectra were acquired every 10 s. As shown in Fig. 1a, once switching the potential from −0.3 V_{RHE} to OCP, the metallic Cu was rapidly oxidized to Cu_2O species within 10 s, and its three characteristic bands at 146, ~520, and ~620 cm^{-1} re-appeared after 20 s[28,30,31]. This rapid reoxidation phenomenon indicates a strongly oxidative species existing in the $KHCO_3$ electrolyte, in contrast to the non-reoxidation process of OD-Cu in the Ar-saturated 0.25 M K_2SO_4 electrolyte (Supplementary Fig. 6). Here K_2SO_4 was selected as a control electrolyte because of its moderate solubility relative to $KClO_4$ (~0.12 M), suitable chemical stability, and relatively weaker interaction with Cu in contrast to such as KCl and KI.

To further confirm the reduction/reoxidation phenomenon, we implemented a loop test where alternate potentials between OCP for 20 s and −0.3 V_{RHE} for 10 s were employed. As shown in Fig. 1b, during the five cycles, we observed that the Cu_2O phase disappears at −0.3 V_{RHE} and re-produces at OCP. We found that the surface Cu species go through the process: $Cu_2O \rightarrow CuO_x \rightarrow$ metallic Cu, with the cathode potential decreasing from OCP to −0.3 V_{RHE} (Supplementary Fig. 2). It is a reverse process when switching from −0.3 V_{RHE} to OCP. Thus, we suggest that the

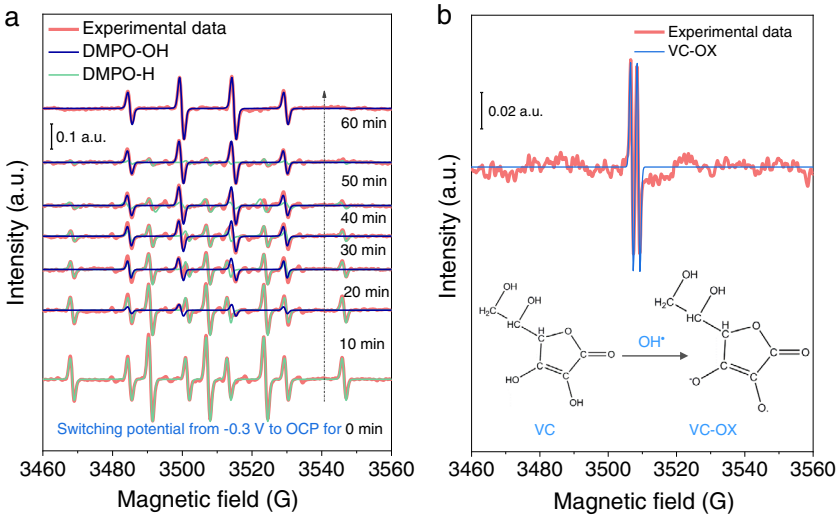

Fig. 2 EPR spectra were recorded in a CO_2-saturated 0.5 M $KHCO_3$ electrolyte containing 100 mM DMPO. a Time-dependent EPR spectra of the $KHCO_3$ solution after switching potential from −0.3 V_{RHE} (20 min reduction) to OCP for different periods. **b** EPR spectra of the $KHCO_3$ solution with 10 mM VC. Inset shows the structure transition from VC and oxidized VC-OX caused by OH•. The simulated EPR spectra of DMPO-OH, DMPO-H, and VC-OX adducts were obtained according to their hyperfine splitting constants.

chemical state of Cu and the phase of surface Cu species are the results of dynamic equilibrium between the cathodic reduction and the reoxidation caused by strongly oxidative species in $KHCO_3$ electrolytes. This explanation may reconcile the debates on the stability of $Cu^{\delta+}$ species during CO_2RR observed from different groups[8,9,16–23].

To preclude the effect of trace undesired oxidative species, such as residual O_2, in the electrolyte or at the electrode surface, we implemented a long-time reduction of electrodeposited Cu electrode in CO_2-saturated $KHCO_3$ solution at −0.3 V_{RHE} for 20 min. Then we switched the potential to OCP while recording the time-dependent optical microscopic images of the electrode surface (Supplementary Fig. 7). Within 10 min, the bright Cu surface gradually converted into a light-black surface, indicating an explicit oxidation process of Cu in the bulk $KHCO_3$ electrolyte.

OH• radicals in $KHCO_3$ electrolytes. Inspired by the formation of various radicals in the $KHCO_3$ system[33–37], we speculate that there may be free radicals in the as-used $KHCO_3$ electrolytes. Thus, EPR spectroscopy was applied to investigate the radical species in a 0.5 M $KHCO_3$ aqueous solution. Considering the very short lifetimes of radicals (up to several ms), 5,5-dimethyl-1-pyrroline N-oxide (DMPO) as a spin trapping agent was added into $KHCO_3$ electrolytes, thus the formed DMPO-radical adducts have the lifetimes as long as minute-scale[38], facilitating the EPR tests.

To eliminate any pre-introduced oxidative species, a 20 min of long-time reduction on the Cu electrode at −0.3 V_{RHE} was performed in CO_2-saturated 0.5 M $KHCO_3$ containing 100 mM DMPO. At −0.3 V_{RHE}, the hydrogen evolution reaction (HER) occurs and the generated hydrogen radicals (H•) can be trapped as a DMPO-H adduct (hyperfine splitting constants, $A_N = 1.65$ mT, $A_H = 2.25$ mT)[38]. Once the potential was switched to OCP, immediately the radicals in the solution were tested through a real-time EPR. As shown in Fig. 2a, DMPO-H radical adduct generated during the HER did not disappear as soon as we stopped the bias, owing to the increased lifetime, thus they can be measured even if we switched the potential from −0.3 V_{RHE} to OCP. Interestingly, after 10 min, the DMPO-OH ($A_N = 1.50$ mT, $A_H = 1.48$ mT)[39] emerged and gradually became the dominant signal with increasing the time within 60 min. Based on this carefully designed test protocol, we claim that the newly generated OH• radicals were indeed activated in the HCO_3^- electrolyte. The continuously ascending OH• radical intensity was further confirmed when resting the $KHCO_3$ solution at OCP for 24 h without pre-reduction at −0.3 V_{RHE} (Supplementary Fig. 8).

We assume that the generation of fresh H• radical will end once stopping the potential at −0.3 V_{RHE}, thus it is reasonable that the DMPO-H signal decays owing to its limited lifetime (Fig. 2a). In contrast, the signal of DMPO-OH increased over 24 h (Supplementary Fig. 8), suggesting a continuous production of OH• radicals with a considerable amount excited by the electrolyte, considering its half-time of DMPO-OH adduct (minute-scale)[40,41]. Besides, the Raman vibration of Cu-OH mode at 710 cm^{-1}, which could be caused by OH• radical, was observed during CO_2RR from 0.2 to −0.3 V_{RHE} (Supplementary Fig. 2)[28,42]. OH• radical is a strongly oxidative species, with a high electrode potential of 2.73 V versus normal hydrogen electrode[43], which can lead to the rapid reoxidation of surface OD-Cu in $KHCO_3$ electrolytes during CO_2RR.

The control experiments showed that no relevant DMPO-OH signals were detected in both pure water and 0.25 M K_2SO_4 solutions containing 100 mM DMPO (Supplementary Fig. 9). Meanwhile, the reoxidation behavior of surface OD-Cu in 0.25 M K_2SO_4 electrolytes was not observed via the in situ Raman test (Supplementary Fig. 6). These results imply that pure water or K^+ cations alone cannot produce OH• radicals at room temperature. Nevertheless, we found that HCO_3^- anions play a key role in the generation of OH• radicals, by tuning the HCO_3^-/SO_4^{2-} mole ratio under the same K^+ concentration (0.5 M), where the DMPO-OH signals decreased with decreasing the HCO_3^- concentrations (Supplementary Fig. 10).

To further verify the OH• radicals, we added 10 mM vitamin C (VC) as an OH• scavenger into the CO_2-saturated 0.5 M $KHCO_3$ solution containing 100 mM DMPO. As shown in Fig. 2b, the EPR signal of the DMPO-OH adduct disappeared and was replaced by a newly formed VC-OX radical ($A_H = 0.18$ mT) that is from VC oxidation (VC-OX) by OH• radicals[44]. The inset in Fig. 2b displays the oxidation process. The oxidation phenomenon was further demonstrated via the color variation of VC

$KHCO_3$ solution from colorless to light yellow after 24 h aging (Supplementary Fig. 11). A control experiment excludes the VC-OX radicals from self-oxidation, where no EPR signals were observed in the 10 mM VC water solution containing 100 mM DMPO (Supplementary Fig. 12). Besides, the reoxidation of OD-Cu electrode at OCP was not observed after the reduction of surface Cu_2O species to metallic Cu at −0.3 V_{RHE} in the CO_2-saturated $KHCO_3$ solution containing VC, by using in situ Raman spectroscopy (Supplementary Fig. 13).

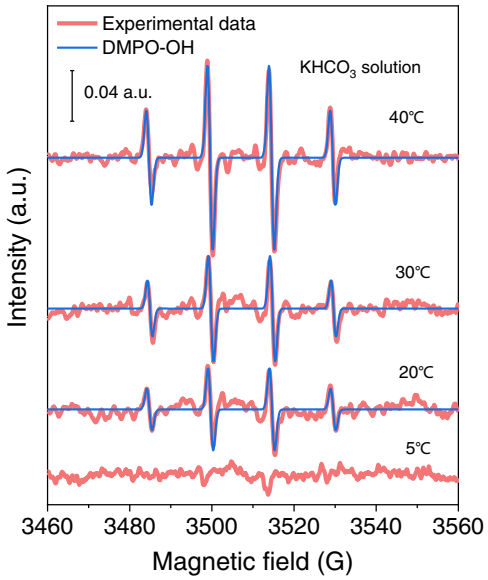

Fig. 3 Temperature-dependent EPR spectra from 5 to 40 °C. EPR data were recorded in Ar-saturated 0.5 M $KHCO_3$ solutions containing 100 mM DMPO without pre-reduction operations. Each spectrum was acquired after 8 h resting at the indicated temperature.

To consider whether the formation of OH• radicals could be a thermally activated process, the signal of the DMPO-OH adduct has been tracked via a temperature-dependent study. We hypothesize that the room temperature may activate HCO_3^- solutions to produce OH• radicals. To confirm it, we implemented the temperature-dependent EPR measurements from 5 to 40 °C in an Ar-saturated 0.5 M $KHCO_3$ electrolyte containing 100 mM DMPO (Fig. 3). When the temperature is as low as 5 °C, no EPR signals were detected. An obvious EPR signal from DMPO-OH was observed around 20 °C and increased with the enhanced temperature. This result indicates that temperature is a key parameter for OH• radical generation in the $KHCO_3$ solutions.

Oxidizing corrosion of Cu plate in $KHCO_3$ solution. Given the steady generation of OH• radicals in $KHCO_3$ electrolytes, we supposed that it would result in a higher degree of oxidizing corrosion of Cu metal. A polished Cu plate (inset in Fig. 4a) was placed into a CO_2-saturated $KHCO_3$ solution. After 24 h resting, a visually light-black Cu surface was observed (inset in Fig. 4b). To preclude the CO_2(aq) effect, the same operation was implemented in Ar-saturated $KHCO_3$, and a darker Cu surface was observed associated with a stronger DMPO-OH signal (inset in Fig. 4c). Thus, the Cu oxidation by CO_2(aq) was ruled out. To further ascertain Cu oxidation by electrolyte-induced OH•, the

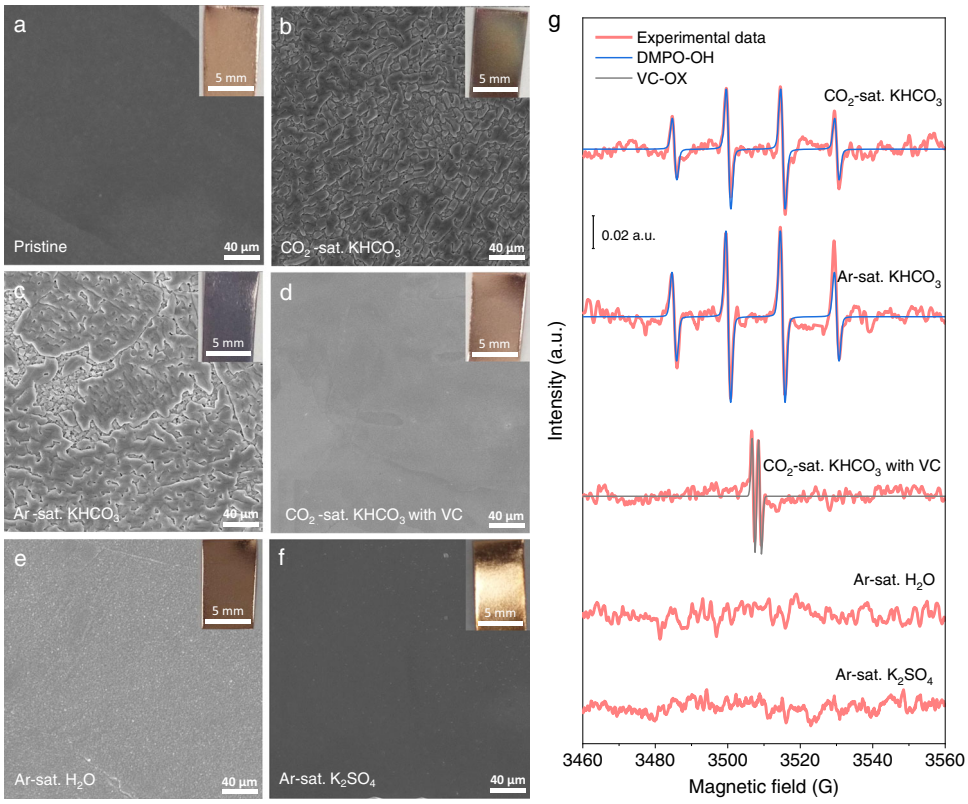

Fig. 4 Oxidizing corrosion of the polished Cu plates in different solutions. SEM images of Cu plates before **a**, and after 24 h oxidizing corrosions in **b** CO_2-saturated $KHCO_3$, **c** Ar-saturated $KHCO_3$, **d** CO_2-saturated $KHCO_3$ containing VC, **e** Ar-saturated ultrapure water, and **f** Ar-saturated K_2SO_4 solutions. Correspondingly, the photographs are displayed in insets. **g** EPR spectra of the corresponding solutions containing 100 mM DMPO after 24 h resting. The concentrations of $KHCO_3$, K_2SO_4, and VC are 0.5 M, 0.25 M, and 10 mM, respectively.

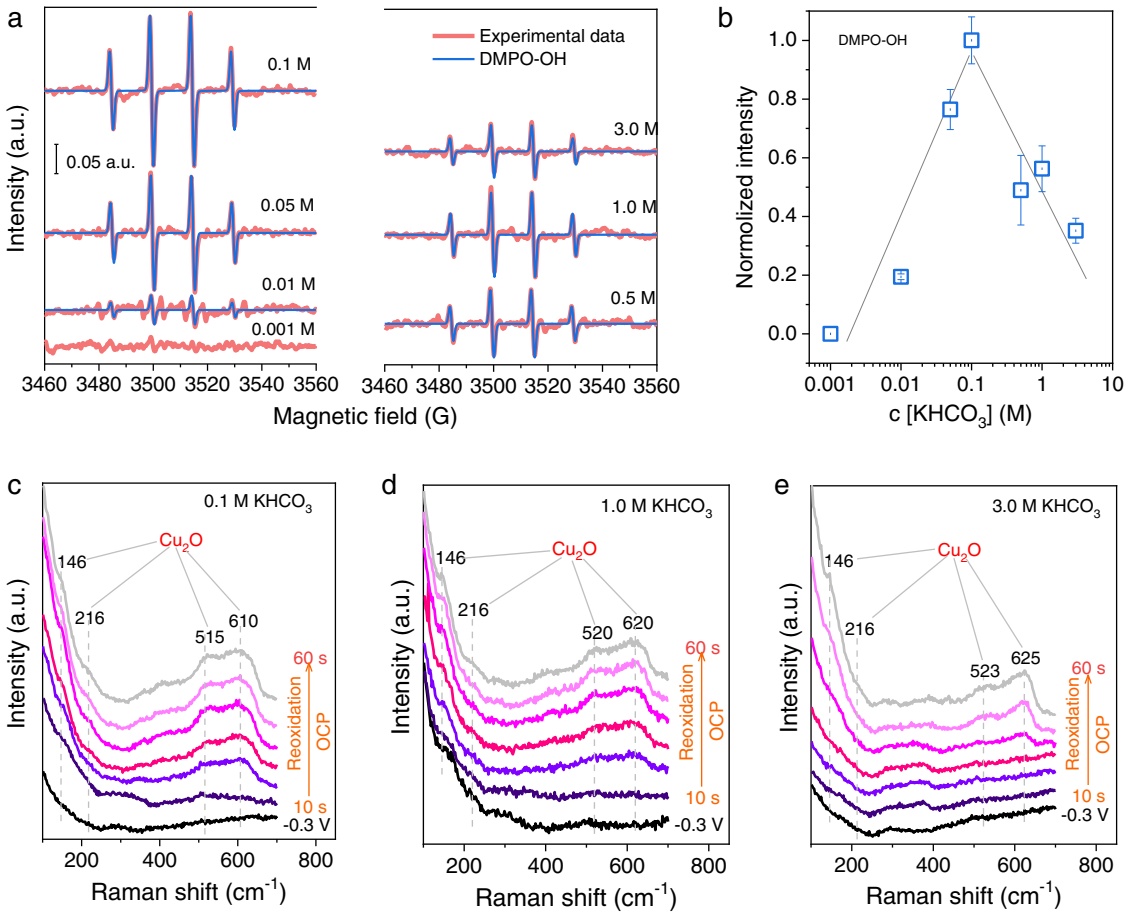

Fig. 5 Relationships between HCO_3^- concentration, OH• radical amount, and reoxidation dynamics of OD-Cu electrodes. a The acquired EPR spectra in different HCO_3^- concentrations. Each solution contains 100 mM DMPO. **b** Correspondingly, the normalized intensity of DMPO-OH versus HCO_3^- concentration. The intensity was normalized by that of 0.1 M HCO_3^-. The gray lines guide the trends of DMPO-OH intensity without the compensation of K^+. The error bars represent the standard deviation. **c**–**e** Raman spectra of OD-Cu reoxidation in different $KHCO_3$ concentrations at OCP after reduction at −0.3 V_{RHE}.

control experiments were carried out in $KHCO_3$ solution containing VC, pure water, and K_2SO_4 solution, respectively. No obvious color changes were visually seen for the three cases (insets in Fig. 4d–f), compared to the pristine Cu plate (inset in Fig. 4a).

The surface morphology of polished Cu plates before and after oxidizing corrosions was characterized by using an optical microscope (Supplementary Fig. 14) and scanning electron microscopy (SEM, Fig. 4a–f). The oxidized surfaces were observed in CO_2- and Ar-saturated $KHCO_3$ solutions (Fig. 4b, c), relative to pristine Cu (Fig. 4a), $KHCO_3$ solution with VC (Fig. 4d), pure water (Fig. 4e), and K_2SO_4 solution (Fig. 4f). Moreover, SEM images showed that the thicknesses of oxide layers at Cu plates reach ~596 and ~780 nm in CO_2- and Ar-saturated $KHCO_3$ solutions, respectively (Supplementary Fig. 15). The phase analyses by X-ray diffraction (Supplementary Fig. 16) and high-resolution transmission electron microscopy (HRTEM, Supplementary Fig. 17) illustrated that the corrosion products mainly consist of Cu_2O. After corrosions, the atomic content of the O element determined by energy-dispersive spectroscopy (Supplementary Figs. 18–23) increased from pristine 0.65% to 14.72% and 19.82% in CO_2- and Ar-saturated $KHCO_3$ solutions respectively, while no obvious variations were discerned for the other three cases (Supplementary Fig. 24).

The oxidizing corrosion degrees are well related to the amount of OH• radicals. As shown in Fig. 4g, after 24 h resting, the CO_2- and Ar-saturated $KHCO_3$ solutions display obvious EPR signals of DMPO-OH and the latter has a higher intensity. By comparison, there was no signal for the other three solutions, except for the $KHCO_3$ solution with VC that presents an EPR signal of VC-OX due to VC oxidation by OH• radicals. These results are further supported by analyzing the surface chemical states of Cu 2*p* of oxidized Cu plates using X-ray photoelectron spectroscopy (XPS), where a little Cu^{2+} species with deep oxidation was found for CO_2- and Ar-saturated $KHCO_3$ solutions, while only Cu^{1+}/Cu^0 species were identified for the other cases (Supplementary Fig. 25).

Sources of OH• radicals in $KHCO_3$ solutions. According to the above analysis, HCO_3^- anions play a vital role in determining the OH• generation. We thus studied the relationships between HCO_3^- concentration, the intensity of OH• radicals, and reoxidation dynamics on OD-Cu electrodes. Firstly, we investigated the influence of HCO_3^- concentrations on the amount of OH• radicals. As shown in Fig. 5a, at <0.1 M, the DMPO-OH signal increases with increasing the HCO_3^- concentrations, yet further increasing the concentrations cannot produce more OH• radicals. It is worth noting that further increasing the HCO_3^- concentration enhances the K^+ concentration as well. Thus, at the same K^+ concentration (0.5 M) with K^+ compensation by K_2SO_4, the relationship between the HCO_3^- concentration and the intensity of DMPO-OH is more pronounced following the order

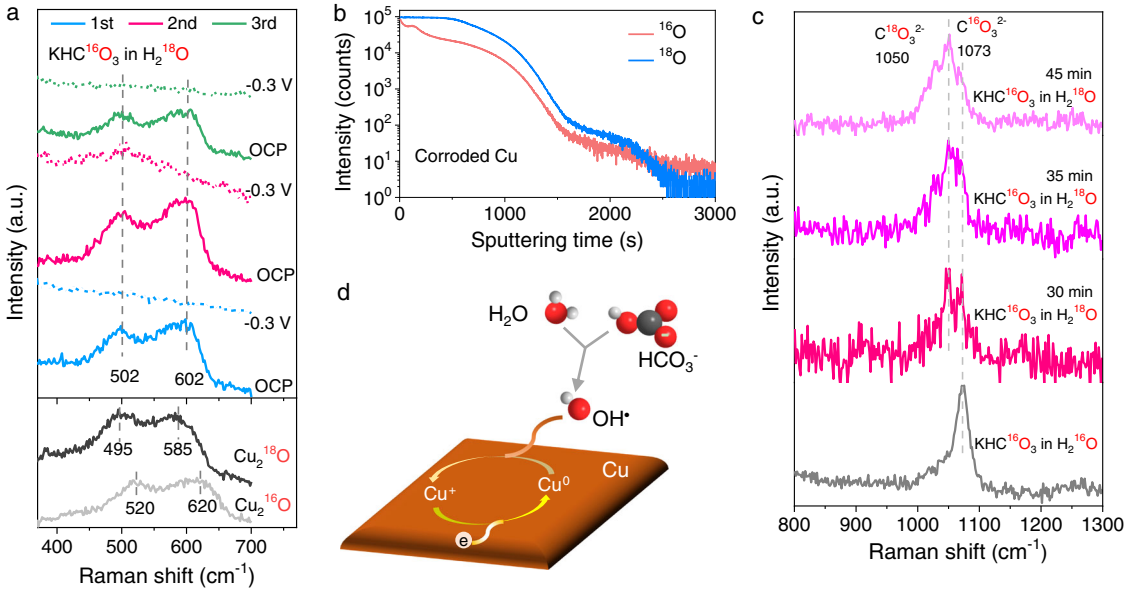

Fig. 6 Determination of OH• sources by oxygen isotope labeling in Ar-saturated 0.5 M $KHC^{16}O_3$ $H_2{}^{18}O$ solution. a Raman spectra of surface Cu_2O species under the loop tests with reduction at −0.3 V_{RHE} for 10 s and subsequently reoxidation at OCP for 20 s. The plots at the bottom show reference spectra for $Cu_2{}^{16}O$ and $Cu_2{}^{18}O$. **b** ^{16}O and ^{18}O contents of the CuO_x species at the Cu plates after 24 h oxidizing corrosion, measured by TOF-SIMS. **c** Raman spectra of carbonate species on the Cu electrode. Each spectrum was obtained after resting the solution for the indicated time. The bottom spectrum shows $C^{16}O_3{}^{2-}$ vibration as a reference. **d** The proposed dynamic reduction/reoxidation process of surface OD-Cu during CO_2RR.

0.2 M < 0.4 M ≤ 0.5 M (Supplementary Fig. 10), and the intensity of DMPO-OH tends to saturate. The optimal HCO_3^- concentration without K^+ compensation for the OH• radical formation is around 0.1 M (Fig. 5b).

Then, to correlate the OH• radicals with reoxidation of OD-Cu electrodes, we carried out in situ Raman in different concentrations of HCO_3^- solutions. As shown in Fig. 5c–e, with increasing the HCO_3^- concentration from 0.1 to 3.0 M, the Raman intensity of Cu_2O species decreases, and the reappearance of Cu_2O phase delays, during the reoxidation processes after reduction at −0.3 V_{RHE}. Thus, it is indeed that the intensity of DMPO-OH is very related to the reoxidation ability. These results suggest that HCO_3^- contributes to the generation of OH• radicals that oxidize the Cu surfaces.

To clarify the sources of OH• radicals, we applied a Raman measurement with oxygen isotope labeling in Ar-saturated 0.5 M $KHC^{16}O_3$ $H_2{}^{18}O$ solution. The Raman vibrations of surface Cu_2O species were recorded again by applying alternate potentials between −0.3 V_{RHE} and OCP. As shown in Fig. 6a, during the three cycles, the characteristic bands of Cu_2O species at ~502 and ~602 cm^{-1} locate between those of $Cu_2{}^{16}O$ (520, 620 cm^{-1}) and $Cu_2{}^{18}O$ (495, 585 cm^{-1}). This indicates that both $HC^{16}O_3^-$ anions and $H_2{}^{18}O$ are responsible for the OH• generation.

To further reveal the respective contributions of $HC^{16}O_3^-$ and $H_2{}^{18}O$ to OH• radicals, we implemented time-of-flight secondary-ion mass spectrometry (TOF-SIMS) measurement to investigate the ^{16}O and ^{18}O contents of CuO_x species formed after 24 h oxidizing corrosion of Cu plate in Ar-saturated 0.5 M $KHC^{16}O_3$ $H_2{}^{18}O$ solution. As illustrated in Fig. 6b, both ^{16}O and ^{18}O are detected in the whole sampling depth, and the latter has a little higher content. Concerning that pure water does not donate OH• radicals (Fig. 4g and Supplementary Fig. 9), and the isotope oxygen mole ratio ($HC^{16}O_3^-$ over $H_2{}^{18}O$ is around 1:100), we hypothesize that oxygen exchange between $H_2{}^{18}O$ and $HC^{16}O_3^-$ may exist.

To support this hypothesis, we tracked the adsorbed carbonate species on the OD-Cu electrode in Ar-saturated $KHC^{16}O_3$ $H_2{}^{18}O$ solution by using Raman spectroscopy. As displayed in Fig. 6c, within 30 min, both $C^{16}O_3{}^{2-}$ vibration from pristine $HC^{16}O_3^-$ at 1073 cm^{-1} and $C^{18}O_3{}^{2-}$ vibration from ^{18}O-derived $HC^{18}O_3^-$ at 1050 cm^{-1} were detected[45], indicating a fast oxygen exchange. After 45 min, dominant $C^{18}O_3{}^{2-}$ vibration from ^{18}O-exchanged $HC^{18}O_3^-$ was observed. Thus, we show that the OH• radicals have been generated at room temperature in HCO_3^- electrolytes while the dynamic oxygen exchange between HCO_3^- and H_2O supplies oxygen sources for the formation of OH• radicals.

Based on the above results, we proposed a mechanism for the dynamic reduction/reoxidation behavior at the OD-Cu surface during CO_2RR in Fig. 6d. The reduction of $Cu^{\delta+}$ species to metallic Cu^0 driven via cathodic reduction competes with the reoxidation of Cu^0 to $Cu^{\delta+}$ state caused by the highly oxidative OH• radicals. Thereby, there is a "seesaw-effect" between the reduction and reoxidation, determining the chemical state of Cu and the content of CuO_x species at the surfaces of Cu electrodes in CO_2RR.

We discovered that strongly oxidative OH• radicals can be easily generated in HCO_3^- aqueous solutions at room temperature, and the fast oxygen exchange between HCO_3^- and H_2O provides dynamic oxygen sources for the OH• radical formation. The generated OH• radicals enable rapid reoxidation of OD-Cu electrodes in $KHCO_3$ electrolytes during CO_2RR. Besides, the continuous generation of OH• radicals can make higher degrees of oxidizing corrosion of Cu electrodes in $KHCO_3$ solutions to form substantial surface CuO_x species relative to those electrolytes without OH• radicals. We further suggest that the dynamic chemical states of Cu and the content of surface CuO_x species are determined by a "seesaw-effect" between the cathodic reduction potentials and the OH• radical-involving oxidation. This work provides insights into the reoxidation mechanism of OD-Cu and a general guide for understanding the crucial role of electrolyte composition for the CO_2RR.

Methods

Electrodeposited Cu electrodes. All the electrochemical operations were performed using a Bio-logic SP200 potentiostat. A modified electrodeposition method was used to deposit micro-nano Cu particles at the Cu mesh substrate[29]. The copper mesh was ultrasonically cleaned in acetone, ethanol, and deionized water in

sequence. After drying by flowing N_2, the electrodeposition was carried out by applying a reduction current of -40 mA cm^{-2} for 20 min to the Cu mesh electrode in an Ar-saturated solution consisting of 0.1 M $CuSO_4{\cdot}5H_2O$ (>99.99%, Aladdin) and 1.5 M H_2SO_4 (>98%, Chron Chemicals). The as-prepared electrode was rinsed with water and ethanol sequentially and then dried under a stream of N_2.

Polished Cu plates. Cu plate with a thickness of ~0.2 mm was first polished by using 3000 mesh sandpaper and then cleaned in acetone, ethanol, and deionized water in sequence. Further, it was electropolished in 85% phosphoric acid (Chron Chemicals) solution at 3.0 V versus counter-electrode of another Cu plate for 5 min. After that, the polished Cu plate was ultrasonically cleaned in Ar-saturated ultrapure water (Milli-Q, 18.2 MΩ) to remove the surface residual particles.

Oxidizing corrosion of polished Cu plates. The polished Cu plates were placed into CO_2-, Ar-saturated 0.5 M $KHCO_3$, CO_2-saturated 0.5 M $KHCO_3$ containing 10 mM VC, Ar-saturated ultrapure water, Ar-saturated 0.25 M K_2SO_4, and Ar-saturated 0.5 M $KHCO_3$ $H_2{}^{18}O$ solutions, respectively. After resting for 24 h, the corrosive Cu plates were rinsed with water and then dried under a stream of N_2.

Materials characterization. Crystal phase structures were characterized by an XRD diffractometer (Equinox 1000, Thermo Fisher Scientific) with Cu Kα radiation ($\lambda = 1.54$ Å). Morphology was observed by field-emission SEM (FEI Inspect F50). Elemental analysis was implemented by using EDS. TEM and HRTEM images were acquired by using an FEI Titan G2 60-300 electron microscope. The surface chemistry of the Cu electrode/plate was investigated using XPS (Thermo ESCALAB 250XI) with Al Kα X-rays (1486.6 eV). The depth ^{16}O and ^{18}O contents of CuO_x species formed at the surface of the Cu plate were analyzed by applying TOF-SIMS (ION TOF-SIMS 5) with 30 keV-Bi_3^+ as an analysis gun and 2 keV-Cs^+ as the sputtering source.

In situ Raman spectroscopy. Raman spectra were recorded with an XploRA PLUS Raman spectrometer (Horiba Jobin Yvon) equipped with a ×50 objective and a 638 nm He-Ne laser. The filter was set at 50%. The measurements were conducted using a custom-made three-electrode electrochemical cell with a quartz window, in which the as-prepared Cu electrode, Ag/AgCl (3.0 M KCl), and membrane-separated Pt wire were used as the working, reference, and counter electrodes. Before each test, the as-used electrolyte was pumped into the cell at a rate of 2 ml min^{-1}. The equipped optical microscope was applied to acquire the real-time microscopic images of as-used Cu electrodes during the Raman tests.

EPR spectroscopy. EPR measurements were carried out using a continuous-wave Bruker EMX micro spectrometer operating in X-band mode with a frequency of 9.848 GHz at room temperature. Each spectrum was recorded using the following parameters: a microwave power of 20 mW, modulation amplitude of 1.0 G, and a single scan with a sweep time of 5 min. DMPO (Dojindo) was selected as the spin trapping agent, and its concentration in all solutions was 100 mM. For EPR measurements taken during electrocatalysis in the presence of a Cu electrode, the electrolyte was immediately measured after electrolysis at a given potential in a specific electrolyte containing 100 mM DMPO. EPR simulations were performed according to the hyperfine splitting constants of radicals, via using the Xenon software provided by the EPR manufacturer.

Data availability

All the data that support the findings of this study are available within the paper and its Supplementary Information files, or from the corresponding author on reasonable request.

Received: 20 November 2021; Accepted: 21 June 2022;
Published online: 27 June 2022

References

1. Nitopi, S. et al. Progress and perspectives of electrochemical CO_2 reduction on copper in aqueous electrolyte. *Chem. Rev.* **119**, 7610–7672 (2019).
2. Fan, L. et al. Strategies in catalysts and electrolyzer design for electrochemical CO_2 reduction toward C_{2+} products. *Sci. Adv.* **6**, eaay3111 (2020).
3. Nguyen, T. N. & Dinh, C. T. Gas diffusion electrode design for electrochemical carbon dioxide reduction. *Chem. Soc. Rev.* **49**, 7488–7504 (2020).
4. Li, C. W. & Kanan, M. W. CO_2 reduction at low overpotential on Cu electrodes resulting from the reduction of thick Cu_2O films. *J. Am. Chem. Soc.* **134**, 7231–7234 (2012).
5. Popovic, S. et al. Stability and degradation mechanisms of copper-based catalysts for electrochemical CO_2 reduction. *Angew. Chem. Int. Ed.* **59**, 14736–14746 (2020).
6. Raciti, D. & Wang, C. Recent advances in CO_2 reduction electrocatalysis on copper. *ACS Energy Lett.* **3**, 1545–1556 (2018).
7. Lee, S. Y. et al. Mixed copper states in anodized Cu electrocatalyst for stable and selective ethylene production from CO_2 reduction. *J. Am. Chem. Soc.* **140**, 8681–8689 (2018).
8. Yang, P. P. et al. Protecting copper oxidation state via intermediate confinement for selective CO_2 electroreduction to C_{2+} fuels. *J. Am. Chem. Soc.* **142**, 6400–6408 (2020).
9. Arán-Ais, R. M., Scholten, F., Kunze, S., Rizo, R. & Roldan Cuenya, B. The role of in situ generated morphological motifs and Cu(I) species in C_{2+} product selectivity during CO_2 pulsed electroreduction. *Nat. Energy* **5**, 317–325 (2020).
10. Favaro, M. et al. Subsurface oxide plays a critical role in CO_2 activation by Cu(111) surfaces to form chemisorbed CO_2, the first step in reduction of CO_2. *Proc. Natl Acad. Sci. USA* **114**, 6706–6711 (2017).
11. Xiao, H., Goddard, W. A. 3rd, Cheng, T. & Liu, Y. Cu metal embedded in oxidized matrix catalyst to promote CO_2 activation and CO dimerization for electrochemical reduction of CO_2. *Proc. Natl Acad. Sci. USA* **114**, 6685–6688 (2017).
12. Shang, L., Lv, X., Shen, H., Shao, Z. & Zheng, G. Selective carbon dioxide electroreduction to ethylene and ethanol by core-shell copper/cuprous oxide. *J. Colloid Interface Sci.* **552**, 426–431 (2019).
13. Zhi, X., Vasileff, A., Zheng, Y., Jiao, Y. & Qiao, S.-Z. Role of oxygen-bound reaction intermediates in selective electrochemical CO_2 reduction. *Energy Environ. Sci.* **14**, 3912–3930 (2021).
14. Wu, Z.-Z., Gao, F.-Y. & Gao, M.-R. Regulating the oxidation state of nanomaterials for electrocatalytic CO_2 reduction. *Energy Environ. Sci.* **14**, 1121–1139 (2021).
15. Beverskog, B. & Puigdomenech, I. Revised Pourbaix diagrams for copper at 25 to 300°C. *J. Electrochem. Soc.* **144**, 3476–3483 (1997).
16. Permyakova, A. A. et al. On the oxidation state of Cu_2O upon electrochemical CO_2 reduction: an XPS study. *Chemphyschem* **20**, 3120–3127 (2019).
17. Moller, T. et al. Electrocatalytic CO_2 reduction on CuO_x nanocubes: tracking the evolution of chemical state, geometric structure, and catalytic selectivity using operando spectroscopy. *Angew. Chem. Int. Ed.* **59**, 17974–17983 (2020).
18. Lee, S. H. et al. Oxidation state and surface reconstruction of Cu under CO_2 reduction conditions from in situ X-ray characterization. *J. Am. Chem. Soc.* **143**, 588–592 (2021).
19. Lei, Q. et al. Investigating the origin of enhanced C_{2+} selectivity in oxide-/hydroxide-derived copper electrodes during CO_2 electroreduction. *J. Am. Chem. Soc.* **142**, 4213–4222 (2020).
20. Farmand, M. et al. Electrochemical flow cell enabling operando probing of electrocatalyst surfaces by X-ray spectroscopy and diffraction. *Phys. Chem. Chem. Phys.* **21**, 5402–5408 (2019).
21. De Luna, P. et al. Catalyst electro-redeposition controls morphology and oxidation state for selective carbon dioxide reduction. *Nat. Catal.* **1**, 103–110 (2018).
22. Kim, D. et al. Insights into an autonomously formed oxygen-evacuated Cu_2O electrode for the selective production of C_2H_4 from CO_2. *Phys. Chem. Chem. Phys.* **17**, 824–830 (2015).
23. Cavalca, F. et al. Nature and distribution of stable subsurface oxygen in copper electrodes during electrochemical CO_2 reduction. *J. Phys. Chem. C.* **121**, 25003–25009 (2017).
24. Mistry, H. et al. Highly selective plasma-activated copper catalysts for carbon dioxide reduction to ethylene. *Nat. Commun.* **7**, 12123 (2016).
25. Chang, C. J. et al. Dynamic reoxidation/reduction-driven atomic interdiffusion for highly selective CO_2 reduction toward methane. *J. Am. Chem. Soc.* **142**, 12119–12132 (2020).
26. Chang, C. J. et al. Quantitatively unraveling the redox shuttle of spontaneous oxidation/electroreduction of CuO_x on silver nanowires using in situ X-ray absorption spectroscopy. *ACS Cent. Sci.* **5**, 1998–2009 (2019).
27. Wang, J., Tan, H. Y., Zhu, Y., Chu, H. & Chen, H. M. Linking the dynamic chemical state of catalysts with the product profile of electrocatalytic CO_2 reduction. *Angew. Chem. Int. Ed.* **60**, 17254–17267 (2021).
28. Zhao, Y. et al. Speciation of Cu surfaces during the electrochemical CO reduction reaction. *J. Am. Chem. Soc.* **142**, 9735–9743 (2020).
29. Wakerley, D. et al. Bio-inspired hydrophobicity promotes CO_2 reduction on a Cu surface. *Nat. Mater.* **18**, 1222–1227 (2019).
30. Chen, X. et al. Controlling speciation during CO_2 reduction on Cu-alloy electrodes. *ACS Catal.* **10**, 672–682 (2019).
31. Jiang, S., Klingan, K., Pasquini, C. & Dau, H. New aspects of operando Raman spectroscopy applied to electrochemical CO_2 reduction on Cu foams. *J. Chem. Phys.* **150**, 041718 (2019).
32. Vavra, J., Shen, T. H., Stoian, D., Tileli, V. & Buonsanti, R. Real-time Monitoring Reveals dissolution/redeposition mechanism in copper nanocatalysts during the initial stages of the CO_2 reduction reaction. *Angew. Chem. Int. Ed.* **60**, 1347–1354 (2021).

33. Draganić, Z. D. et al. Radiolysis of aqueous solutions of ammonium bicarbonate over a large dose range. *Int. J. Radiat. Appl. lnstrum. Part C. Radiat. Phys. Chem.* **38**, 317–321 (1991).
34. Walton, J. C. Radical-enhanced acidity: why bicarbonate, carboxyl, hydroperoxyl, and related radicals are so acidic. *J. Phys. Chem. A* **121**, 7761–7767 (2017).
35. Pan, H. et al. Recent advances in bicarbonate-activated hydrogen peroxide system for water treatment. *Chem. Eng. J.* **408**, 127332 (2021).
36. Gennaro, A. et al. Mechanism of the electrochemical reduction of carbon dioxide at inert electrodes in media of low proton availability. *J. Chem. Soc., Faraday Trans.* **92**, 3963–3968 (1996).
37. Gupta, N., Gattrell, M. & MacDougall, B. Calculation for the cathode surface concentrations in the electrochemical reduction of CO_2 in $KHCO_3$ solutions. *J. Appl. Electrochem.* **36**, 161–172 (2005).
38. Buettner, G. R. Spin trapping: ESR parameters of spin adducts. *Free Radic. Biol. Med.* **3**, 259–303 (1987).
39. Chen, J. et al. OH radicals determined photocatalytic degradation mechanisms of gaseous styrene in TiO_2 system under 254 nm versus 185 nm irradiation: combined experimental and theoretical studies. *Appl. Catal. B-Environ.* **257**, 117912 (2019).
40. Tsai, P., Pou, S., Straus, R. & G. M. Rosen evaluation of various spin traps for the in vivo in situ detection of hydroxyl radical. *J. Chem. Soc. Perkin Trans.* **2**, 1759–1764 (1999).
41. Nakamura, K. et al. Reevaluation of quantitative ESR spin trapping analysis of hydroxyl radical by applying sonolysis of water as a model system. *Bull. Chem. Soc. Jpn.* **83**, 1037–1046 (2010).
42. Bodappa, N. et al. Early stages of electrochemical oxidation of Cu(111) and polycrystalline Cu surfaces revealed by in situ raman spectroscopy. *J. Am. Chem. Soc.* **141**, 12192–12196 (2019).
43. Armstrong, D. A. et al. Standard electrode potentials involving radicals in aqueous solution: inorganic radicals (IUPAC Technical Report). *Pure Appl. Chem.* **87**, 1139–1150 (2015).
44. Dodd, N. J. F. Some EPR signals in tumour tissue. *Br. J. Cancer* **28**, 257–262 (1973).
45. Zhang, Z. et al. pH matters when reducing CO_2 in an electrochemical flow cell. *ACS Energy Lett.* **5**, 3101–3107 (2020).

Acknowledgements

C.C. acknowledges funding support from the Natural Science Foundation of China (22072013). S.M. thanks funding support from the China Postdoctoral Science Foundation (No. 2020M673169).

Author contributions

C.C. supervised the project. S.M. carried out the experiments. H.L. and Q.W. contributed to the EPR measurements and analysis. L.L. and R.Z. contributed to partial Raman measurements. S.M., C.L. and C.C. wrote and revised the manuscript. All authors commented on the manuscript.

Competing interests

The authors declare no competing interests.

Additional information

Supplementary information The online version contains supplementary material available at https://doi.org/10.1038/s41467-022-31498-8.

Correspondence and requests for materials should be addressed to Chang Long or Chunhua Cui.

Peer review information *Nature Communications* thanks Joel Ager III and the other anonymous reviewer(s) for their contribution to the peer review of this work. Peer review reports are available.

Reprints and permission information is available at http://www.nature.com/reprints

Publisher's note Springer Nature remains neutral with regard to jurisdictional claims in published maps and institutional affiliations.